Journal of Sound and Vibration (2000) **232**(5), 897–915
doi:10.1006/jsvi.1999.2775, available online at http://www.idealibrary.com on IDEAL®

ESTIMATION OF VIBRATIONAL POWER IN BUILT-UP SYSTEMS INVOLVING BOX-LIKE STRUCTURES, PART 2: INFINITE TOP-PLATE AND CIRCULAR GEOMETRY

R. A. FULFORD† AND B. A. T. PETERSSON

*AAETS, Loughborough University, Loughborough LE*11 3*TU, England*

(*Received* 15 *March* 1999, *and in final form* 1 *September* 1999)

Following on from a previous paper [1], work is presented in which the distributed forces exhibited between a box and its top and recipient are simplified by the introduction of assumed uniform distributions. The box consists of four side-walls, the recipient is a thick infinite plate, and the model is completed with a thin infinite top-plate attached via a roller condition. The introduction of a *roller coupled infinite* top-plate is motivated by the hypothesis that losses associated with wave propagation into its outlying region equate, approximately, to losses inherent in a *fully coupled finite* top-plate associated with wave conversion (at the coupled boundaries) and then divergence and dissipation (within the structure). Comparisons with experimental results are presented which corroborate the hypothesis. When uniform force distributions are assumed the study indicates that the transmitted power can be reliably calculated up to the first two or three resonances and, for higher wavenumbers, that the overall trend can be predicted. A constraint to this conclusion is, however, that strongly excited, anti-symmetric modes cannot be predicted. Analytical studies in which the box is reduced to a circular can are also performed and the results indicate that this simplification is valid when the requirement is for a simple estimate of the overall trend of the power. Overall, therefore, the paper proposes several possibilities through which models of built-up systems can be simplified.

1. INTRODUCTION

In previous work [1] the analysis of box-like structures was simplified by assuming the forces manifested at the side-wall/top-plate and side-wall/recipient-plate interfaces were uniform. The approach was considered promising since the simplified models proved reliable up to the second longitudinal resonance of the side-walls, provided that the magnitude of the uniform force distributions were the spatial averages of the true distributed forces. In an attempt to develop this finding for practical use, the introduction of an infinite top-plate onto the box is considered (see Figure 1). Whilst initially such a step may appear irregular, it is logical since the box in the previous paper was "incomplete" in that only prescribed force distributions (obtained from a simply supported plate) were imposed on the upper edges of the side-walls. The previous box therefore lacked a coupled top-plate and so the introduction of a top-plate "completes" the box.

The question of why an infinite as opposed to a finite top-plate is introduced is partially answered in reference [2] which suggests that when two plates are coupled perpendicular to each other and the ratio of their thicknesses exceeds 2:1 the effect of moments can, depending upon which plate is thickest, either be ignored or accounted for by a simple

† Present address: Institut für Technische Akustik, Technische Universität Berlin, 10587 Berlin, Germany.

0022-460X/00/200897 + 19 $35.00/0

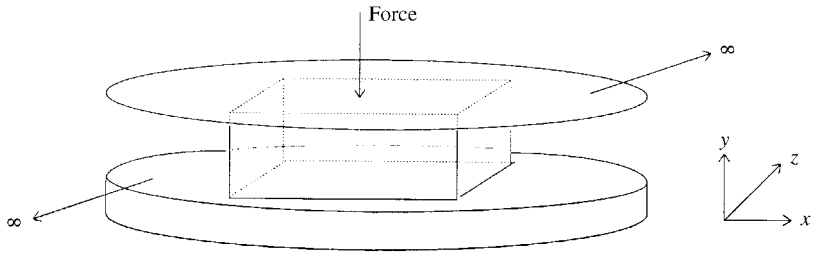

Figure 1. Infinite top-plate of the box.

modification of the boundary condition. Under these conditions the introduction of an infinite top-plate is valid since the moment-induced power propagates to an outlying region and so, in agreement with reference [2], it is essentially omitted from the model. Thus, under the proviso that the ratio of top-plate thickness to side-plate thickness is 2 : 1 or larger an infinite top-plate, attached via a roller condition, can be introduced into the model. When the two plates have the same thickness, moments do however assume importance [2] and the introduction of an infinite top-plate attached via a roller condition has to be examined more closely. Under this condition, it is therefore noted that for a physical box, which has a finite and fully coupled top-plate, much wave conversion occurs at the boundaries (bending wave to in-plane wave and *vice versa*). This is in contrast to the author's simplified model in which only bending waves occur in the top- and recipient-plates and only longitudinal waves occur in the side-walls. Thus, it is conjectured that the losses in a real box associated with dissipation and divergence can equate approximately to the losses in the model associated with the moment-induced power propagating to the outlying region of the infinite top-plate. If this is so the model can be considered equivalent to an actual box.

2. AN INFINITE TOP-PLATE

To model a box sandwiched between two infinite plates a mobility approach can be used. For this method the system is first deconstructed into simplified elements for which mathematical descriptions can be developed and then the built-up structure reconstructed using these elementary components. This technique is useful since it offers an analytical rather than a numerical solution with the subsequent advantage that some insight into the salient physical behaviour of the structure can then be deduced. For the sandwiched box, two elementary components, a side-wall and an infinite plate, are designated as the sub-components of the whole.

As in a previous paper [1] the side-wall is considered to have only in-plane motion and to have a roller condition for its vertical edges. For point excitation its mobility is given by

$$Y(x_1|x_n) = \frac{\mathrm{i}}{l_x} \sum_{m=0}^{\infty} \cos\left(\frac{m\pi x_1}{l_x}\right) Y_\infty\left(\frac{m\pi}{l_x}\right) \cos\left(\frac{m\pi x_n}{l_x}\right), \tag{1}$$

where $Y_\infty(m\pi/l_x)$ is the in-plane mobility of an infinite side-wall [1, 3]. The other symbols are defined in Appendix A.

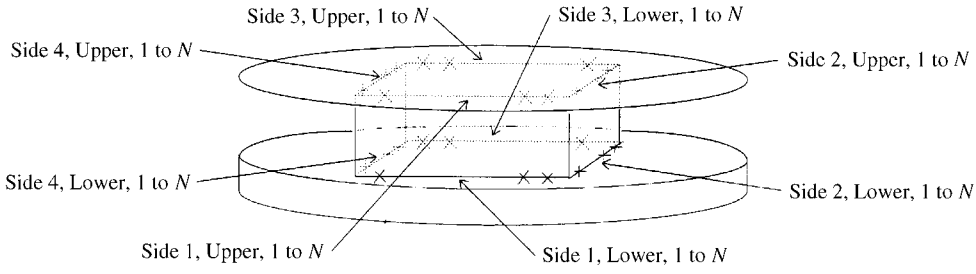

Figure 2. Discretization of all interfaces.

The mobility of the thin infinite plate, subject to transverse point excitation is given in reference [4] as

$$Y(x_1|x_n) = \frac{\omega 12(1-v^2)}{8Eh^3k_B^2}\ [\mathrm{H}_0^{(2)}(k_B r) - \mathrm{H}_0^{(2)}(-\mathrm{i}k_B r)]. \tag{2}$$

With the above mobility functions defined for discrete excitation and response positions, it is convenient to reconstruct the box mathematically using a series of discrete point connections along the line interfaces (see Figure 2). In this manner, the continuous distributions can be synthesized provided that the Nyquist criterion (two points per wavelength) is met. The discrete forces acting at the upper and lower edges of the box can then be determined using

$$\begin{bmatrix} [\mathbf{F}^L_{11}] \\ [\mathbf{F}^L_{22}] \\ [\mathbf{F}^L_{33}] \\ [\mathbf{F}^L_{44}] \\ [\mathbf{F}^U_{11}] \\ [\mathbf{F}^U_{22}] \\ [\mathbf{F}^U_{33}] \\ [\mathbf{F}^U_{44}] \end{bmatrix}$$

$$= \begin{bmatrix} [\mathbf{Y}^L_{s_{11}} + \mathbf{Y}^L_{r_{11}}] & [\mathbf{Y}^L_{r_{21}}] & [\mathbf{Y}^L_{r_{31}}] & [\mathbf{Y}^L_{r_{41}}] & [\mathbf{Y}^{UL}_{s_{11}}] & [\mathbf{0}] & [\mathbf{0}] & [\mathbf{0}] \\ [\mathbf{Y}^L_{r_{12}}] & [\mathbf{Y}^L_{s_{22}} + \mathbf{Y}^L_{r_{22}}] & [\mathbf{Y}^L_{r_{32}}] & [\mathbf{Y}^L_{r_{42}}] & [\mathbf{0}] & [\mathbf{Y}^{UL}_{s_{22}}] & [\mathbf{0}] & [\mathbf{0}] \\ [\mathbf{Y}^L_{r_{13}}] & [\mathbf{Y}^L_{r_{23}}] & [\mathbf{Y}^L_{s_{33}} + \mathbf{Y}^L_{r_{33}}] & [\mathbf{Y}^L_{r_{43}}] & [\mathbf{0}] & [\mathbf{0}] & [\mathbf{Y}^{UL}_{s_{33}}] & [\mathbf{0}] \\ [\mathbf{Y}^L_{r_{14}}] & [\mathbf{Y}^L_{r_{24}}] & [\mathbf{Y}^L_{r_{34}}] & [\mathbf{Y}^L_{s_{44}} + \mathbf{Y}^L_{r_{44}}] & [\mathbf{0}] & [\mathbf{0}] & [\mathbf{0}] & [\mathbf{Y}^{UL}_{s_{44}}] \\ [\mathbf{Y}^{UL}_{s_{11}}] & [\mathbf{0}] & [\mathbf{0}] & [\mathbf{0}] & [\mathbf{Y}^U_{s_{11}} + \mathbf{Y}^U_{t_{11}}] & [\mathbf{Y}^U_{t_{21}}] & [\mathbf{Y}^U_{t_{31}}] & [\mathbf{Y}^U_{t_{41}}] \\ [\mathbf{0}] & [\mathbf{Y}^{UL}_{s_{22}}] & [\mathbf{0}] & [\mathbf{0}] & [\mathbf{Y}^U_{t_{12}}] & [\mathbf{Y}^U_{s_{22}} + \mathbf{Y}^U_{t_{22}}] & [\mathbf{Y}^U_{t_{32}}] & [\mathbf{Y}^U_{t_{42}}] \\ [\mathbf{0}] & [\mathbf{0}] & [\mathbf{Y}^{UL}_{s_{33}}] & [\mathbf{0}] & [\mathbf{Y}^U_{t_{13}}] & [\mathbf{Y}^U_{t_{23}}] & [\mathbf{Y}^U_{s_{33}} + Y^U_{t_{33}}] & [\mathbf{Y}^U_{t_{43}}] \\ [\mathbf{0}] & [\mathbf{0}] & [\mathbf{0}] & [\mathbf{Y}^{UL}_{s_{44}}] & [\mathbf{Y}^U_{t_{14}}] & [\mathbf{Y}^U_{t_{24}}] & [\mathbf{Y}^U_{t_{34}}] & [\mathbf{Y}^U_{s_{44}} + \mathbf{Y}^U_{t_{44}}] \end{bmatrix}^{-1}$$

$$\times \begin{bmatrix} [\mathbf{0}] \\ [\mathbf{0}] \\ [\mathbf{0}] \\ [\mathbf{0}] \\ [\mathbf{Y}^{U0}_{t_{11}}]F^0 \\ [\mathbf{Y}^{U0}_{t_{22}}]F^0 \\ [\mathbf{Y}^{U0}_{t_{33}}]F^0 \\ [\mathbf{Y}^{U0}_{t_{44}}]F^0 \end{bmatrix}, \tag{3}$$

where $[\mathbf{Y}^{L}_{s_{mm}} + \mathbf{Y}^{L}_{r_{mm}}]$ is a sub-matrix designating the summation of the side-wall and recipient mobilities at the lower edge (L) of the side-wall m, and

$$[\mathbf{Y}^{L}_{s_{mm}} + \mathbf{Y}^{L}_{r_{mm}}] = \begin{bmatrix} (\mathbf{Y}^{L^{11}}_{s_{mm}} + \mathbf{Y}^{L^{11}}_{r_{mm}}) & (\mathbf{Y}^{L^{21}}_{s_{mm}} + \mathbf{Y}^{L^{21}}_{r_{mm}}) & \cdots & (\mathbf{Y}^{L^{N1}}_{s_{mm}} + \mathbf{Y}^{L^{N1}}_{r_{mm}}) \\ (\mathbf{Y}^{L^{12}}_{s_{mm}} + \mathbf{Y}^{L^{12}}_{r_{mm}}) & (\mathbf{Y}^{L^{22}}_{s_{mm}} + \mathbf{Y}^{L^{22}}_{r_{mm}}) & \cdots & (\mathbf{Y}^{L^{N2}}_{s_{mm}} + \mathbf{Y}^{L^{N2}}_{r_{mm}}) \\ \cdots & \cdots & \cdots & \cdots \\ (\mathbf{Y}^{L^{1N}}_{s_{mm}} + \mathbf{Y}^{L^{1N}}_{r_{mm}}) & (\mathbf{Y}^{L^{2N}}_{s_{mm}} + \mathbf{Y}^{L^{2N}}_{r_{mm}}) & \cdots & (\mathbf{Y}^{L^{NN}}_{s_{mm}} + \mathbf{Y}^{L^{NN}}_{r_{mm}}) \end{bmatrix}. \tag{4}$$

In Equation (4) N is the number of points in the line discretization and the individual mobility terms for the side-wall $\mathbf{Y}^{Lx,x_n}_{s_{mn}}$ and for the recipient plate $\mathbf{Y}^{Lx,x_n}_{r_{mn}}$ are established from Equations (1) and (2) respectively. Similarly, $[\mathbf{Y}^{L}_{r_{mmx}}]$ is a sub-matrix describing the transfer mobilities of the recipient between the lower edges of side-wall m and n whilst $[\mathbf{Y}^{UL}_{s_{mm}}]$ constitutes the transfer mobilities between the upper and the lower edges of side-wall m. $[\mathbf{Y}^{U}_{t_{mm}}]$ defines the transfer mobilities between the upper edges of the side-walls m and n via the top-plate and $[\mathbf{Y}^{U0}_{t_{mm}}]$ contains the transfer mobilities of the top-plate between the input force and the upper edge of side-wall m. F^0 is the input force and $[\mathbf{F}^{U}_{mm}]$ and $[\mathbf{F}^{L}_{mm}]$ define the forces at the upper and lower edges of side-wall m respectively.

Upon solving for the forces, the power can then be calculated at, for example, the position of the input (excitation) force,

$$Q^0 = \tfrac{1}{2}\{\mathbf{Y}^{00}_{t}\mathbf{F}^0 + [\mathbf{Y}^{U0}_{t_{11}}\mathbf{F}^{U}_{11}] + [\mathbf{Y}^{U0}_{t_{22}}\mathbf{F}^{U}_{22}] + [\mathbf{Y}^{U0}_{t_{33}}\mathbf{F}^{U}_{33}] + [\mathbf{Y}^{U0}_{t_{44}}\mathbf{F}^{U}_{44}]\}\mathbf{F}^{0*}, \tag{5}$$

or, at the lower edge of the box,

$$\begin{aligned} Q^{L}_{nn} = \tfrac{1}{2}\{&[\mathbf{Y}^{UL}_{s_{1n}}\mathbf{F}^{U}_{11}] + [\mathbf{Y}^{UL}_{s_{2n}}\mathbf{F}^{U}_{22}] + [\mathbf{Y}^{UL}_{s_{3n}}\mathbf{F}^{U}_{33}] + [\mathbf{Y}^{UL}_{s_{4n}}\mathbf{F}^{U}_{44}] + [\mathbf{Y}^{L}_{s_{1n}}\mathbf{F}^{L}_{11}] + [\mathbf{Y}^{L}_{s_{2n}}\mathbf{F}^{L}_{22}] \\ &+ [\mathbf{Y}^{L}_{s_{3n}}\mathbf{F}^{L}_{33}] + [\mathbf{Y}^{L}_{s_{4n}}\mathbf{F}^{L}_{44}]\}[\mathbf{F}^{L*}_{nn}]. \end{aligned} \tag{6}$$

Where the forces acting at both the upper and lower interfaces of the side-walls are simplified to have a uniform distribution (see Figure 3), an effective strip mobility approach [5] can be introduced to simplify the above formulations (see reference [1]).

For the side-walls the effective strip mobilities are defined by

$$Y^{\Sigma U,L,UL}_{s_{mm}} = \frac{\displaystyle\int_C F^{U,L,UL}_{mm}(p) \int_{C'} F^{U,L,UL}_{mm}(p')\, Y^{U,L,UL}_{s_{mm}}(p|p')\,\mathrm{d}p\,\mathrm{d}p'}{\left(\displaystyle\int_C F^{U,L,UL}_{mm}(p)\,\mathrm{d}p\right)^2}, \quad p, p' \in [x, z], \quad c, c' \in [l_x, l_z], \tag{7}$$

where for side-wall m, $Y^{U,L,UL}_{s_{mm}}(p|p')$ is the mobility at either the upper (U) or lower (L) interface or the mobility across (UL) the side-wall. The double integral is along the direction x for side-walls 1 and 3 and along z for side-walls 2 and 4.

For the recipient plate, the effective strip mobilities are

$$Y^{\Sigma L}_{r_{mn}} = \frac{\displaystyle\int_C F^{L}_{mn}(p) \int_{C'} F^{L}_{mn}(p')\, Y^{L}_{r_{mn}}(p|p')\,\mathrm{d}p\,\mathrm{d}p'}{\left(\displaystyle\int_C F^{L}_{mn}(p)\,\mathrm{d}p\right)^2}, \quad p, p' \in [x, z], \quad c, c' \in [l_x, l_z], \tag{8}$$

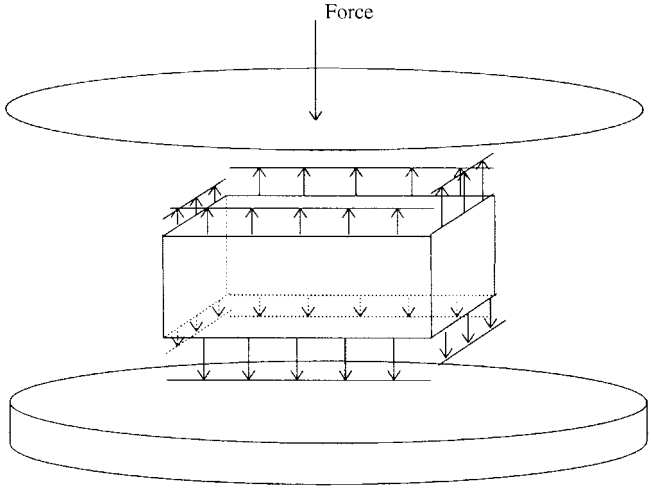

Figure 3. Uniform force distributions along each of the edges.

where $Y^L_{r_{mn}}(p|p')$ is either the mobility along the interface m or between the interfaces m and n.

For the top-plate, two sets of effective strip mobilities are needed, one to describe the interfaces along the side-walls and the other to describe the transfer through the top-plate from the input force to the side-wall. The former are given by

$$Y^{\Sigma U}_{t_{mn}} = \frac{\displaystyle\int_C F^U_{mn}(p) \int_{C'} F^U_{mn}(p')\, Y^U_{t_{mn}}(p|p')\, \mathrm{d}p\, \mathrm{d}p'}{\left(\displaystyle\int_C F^U_{mn}(p)\, \mathrm{d}p\right)^2}, \quad p, p' \in [x, z], \quad c, c' \in [l_x, l_z], \tag{9}$$

and the latter, for a point input force and thus involving only one integral, by

$$Y^{\Sigma U0}_{t_{mm}} = \frac{\displaystyle\int_C F^U_{mm}(p)\, Y^U_{t_{mn}}(p)\, \mathrm{d}p}{\displaystyle\int_C F^U_{mm}(p)\, \mathrm{d}p}, \quad p \in [x, z], \quad c \in [l_x, l_z]. \tag{10}$$

Using the effective strip mobilities, an expression analogous to equation (3) can be developed:

$$\begin{bmatrix} F^L_{11} \\ F^L_{22} \\ F^L_{33} \\ F^L_{44} \\ F^U_{11} \\ F^U_{22} \\ F^U_{33} \\ F^U_{44} \end{bmatrix}$$

$$= \begin{bmatrix} Y^{\Sigma L}_{s_{11}} + Y^{\Sigma L}_{r_{11}} & Y^{\Sigma L}_{r_{21}} & Y^{\Sigma L}_{r_{31}} & Y^{\Sigma L}_{r_{41}} & Y^{\Sigma UL}_{s_{11}} & 0 & 0 & 0 \\ Y^{\Sigma L}_{r_{12}} & Y^{\Sigma L}_{s_{22}} + Y^{\Sigma L}_{r_{22}} & Y^{\Sigma L}_{r_{32}} & Y^{\Sigma L}_{r_{42}} & 0 & Y^{\Sigma UL}_{s_{22}} & 0 & 0 \\ Y^{\Sigma L}_{r_{13}} & Y^{\Sigma L}_{r_{23}} & Y^{\Sigma L}_{s_{33}} + Y^{\Sigma L}_{r_{33}} & Y^{\Sigma L}_{r_{43}} & 0 & 0 & Y^{\Sigma UL}_{s_{33}} & 0 \\ Y^{\Sigma L}_{r_{14}} & Y^{\Sigma L}_{r_{24}} & Y^{\Sigma L}_{r_{34}} & Y^{\Sigma L}_{s_{44}} + Y^{\Sigma L}_{r_{44}} & 0 & 0 & 0 & Y^{\Sigma UL}_{s_{44}} \\ Y^{\Sigma UL}_{s_{11}} & 0 & 0 & 0 & Y^{\Sigma U}_{s_{11}} + Y^{\Sigma U}_{t_{11}} & Y^{\Sigma U}_{t_{21}} & Y^{\Sigma U}_{t_{31}} & Y^{\Sigma U}_{t_{41}} \\ 0 & Y^{\Sigma UL}_{s_{22}} & 0 & 0 & Y^{\Sigma U}_{t_{12}} & Y^{\Sigma U}_{s_{22}} + Y^{\Sigma U}_{t_{22}} & Y^{\Sigma U}_{t_{32}} & Y^{\Sigma U}_{t_{42}} \\ 0 & 0 & Y^{\Sigma UL}_{s_{33}} & 0 & Y^{\Sigma U}_{t_{13}} & Y^{\Sigma U}_{t_{23}} & Y^{\Sigma U}_{s_{33}} + Y^{\Sigma U}_{t_{33}} & Y^{\Sigma U}_{t_{43}} \\ 0 & 0 & 0 & Y^{\Sigma UL}_{s_{44}} & Y^{\Sigma U}_{t_{14}} & Y^{\Sigma U}_{t_{24}} & Y^{\Sigma U}_{t_{34}} & Y^{\Sigma U}_{s_{44}} + Y^{\Sigma U}_{t_{44}} \end{bmatrix}^{-1}$$

$$\times \begin{bmatrix} 0 \\ 0 \\ 0 \\ 0 \\ Y^{\Sigma U0}_{t_{11}} F^0 \\ Y^{\Sigma U0}_{t_{22}} F^0 \\ Y^{\Sigma U0}_{t_{33}} F^0 \\ Y^{\Sigma U0}_{t_{44}} F^0 \end{bmatrix}, \tag{11}$$

where the magnitudes of the spatially assumed uniform force distributions are determined rather than the distributed forces along the interface.

Using the effective strip mobility formulation, the expressions analogous to equations (5) and (6) (i.e. from which the estimates of the input power and the power through the lower edge of the box can be calculated) are found to be

$$Q^0 = \tfrac{1}{2}\{Y^{00}_t F^0 + Y^{U0}_{t_{11}} F^U_{11} + Y^{U0}_{t_{22}} F^U_{22} + Y^{U0}_{t_{33}} F^U_{33} + Y^{U0}_{t_{44}} F^U_{44}\} F^{0*} \tag{12}$$

and

$$Q^L_{nn} = \tfrac{1}{2}\{Y^{\Sigma UL}_{s_{1n}} F^U_{11} + Y^{\Sigma UL}_{s_{2n}} F^U_{22} + Y^{\Sigma UL}_{s_{3n}} F^U_{33} + Y^{\Sigma UL}_{s_{4n}} F^U_{44} + Y^{\Sigma L}_{s_{1n}} \mathbf{F}^L_{11} + Y^{\Sigma L}_{s_{2n}} F^L_{22} + Y^{\Sigma L}_{s_{3n}} F^L_{33} + Y^{\Sigma L}_{s_{4n}} F^L_{44}\} F^{L*}_{nn} \tag{13}$$

respectively. Accordingly, such a formulation becomes equivalent to a four-point coupling problem.

In addition to the simplification of a unique uniform distribution acting at the upper and lower interfaces of each of the side-walls, a greater simplification can be introduced in which the same uniform force distribution is considered to act upon all four of the side-walls simultaneously (see Figure 4). In this case, an overall effective strip mobility has to be defined to account for all of the coupling between all of the four interfaces. This can be achieved easily by extending the integrations of the above effective strip mobilities to encompass the entire perimeter of the box that is

$$Y^{O\Sigma U, L, UL}_s = \frac{\displaystyle\int_C F^{U,L,UL}(p) \int_{C'} F^{U,L,UL}(p') Y^{U,L,UL}_s(p|p') \,\mathrm{d}p \,\mathrm{d}p'}{\left(\displaystyle\int_C F^{U,L,UL}(p) \,\mathrm{d}p\right)^2},$$

$$p, p' \in [x, z], \quad c, c' \in [\text{perimeter}], \tag{14}$$

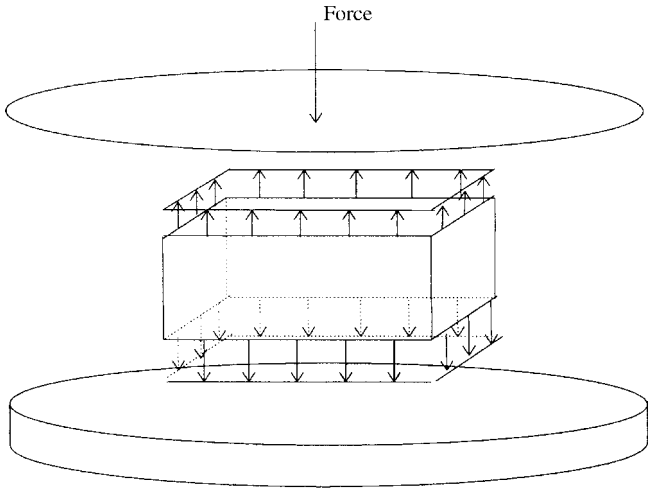

Figure 4. Uniform force distribution around the perimeter.

$$Y_r^{O\Sigma L} = \frac{\int_C F^L(p) \int_{C'} F^L(p') Y_r^L(p|p') \, \mathrm{d}p \, \mathrm{d}p'}{\left(\int_C F^L(p) \, \mathrm{d}p \right)^2}, \quad p, p' \in [x, z], \quad c, c' \in [\text{perimeter}], \tag{15}$$

$$Y_t^{O\Sigma U} = \frac{\int_C F^U(p) \int_{C'} F^U(p') Y_t^U(p|p') \, \mathrm{d}p \, \mathrm{d}p'}{\left(\int_C F^U(p) \, \mathrm{d}p \right)^2}, \quad p, p' \in [x, z], \quad c, c' \in [\text{perimeter}], \tag{16}$$

and

$$Y_{t_{mn}}^{O\Sigma U0} = \frac{\int_C F^U(p) Y_t^{U0}(p) \, \mathrm{d}p}{\int_C F^U(p) \, \mathrm{d}p}, \quad p \in [x, z], \quad c \in [\text{perimeter}]. \tag{17}$$

Analogous to equations (3) and (11) the estimated uniform force magnitudes are then given by

$$\begin{bmatrix} F^L \\ F^U \end{bmatrix} = \begin{bmatrix} (Y_s^{O\Sigma L} + Y_r^{O\Sigma L}) & Y_s^{O\Sigma UL} \\ Y_s^{O\Sigma UL} & (Y_s^{O\Sigma UU} + Y_r^{O\Sigma UU}) \end{bmatrix}^{-1} \times \begin{bmatrix} 0 \\ Y_t^{O\Sigma U0} F^0 \end{bmatrix} \tag{18}$$

and the expressions for the input power and for the power through the lower edge of the side-walls reduce to

$$Q^0 = \tfrac{1}{2} \{ Y_t^{00} F^0 + Y_t^{O\Sigma U0} F^U \} F^{0*}, \tag{19}$$

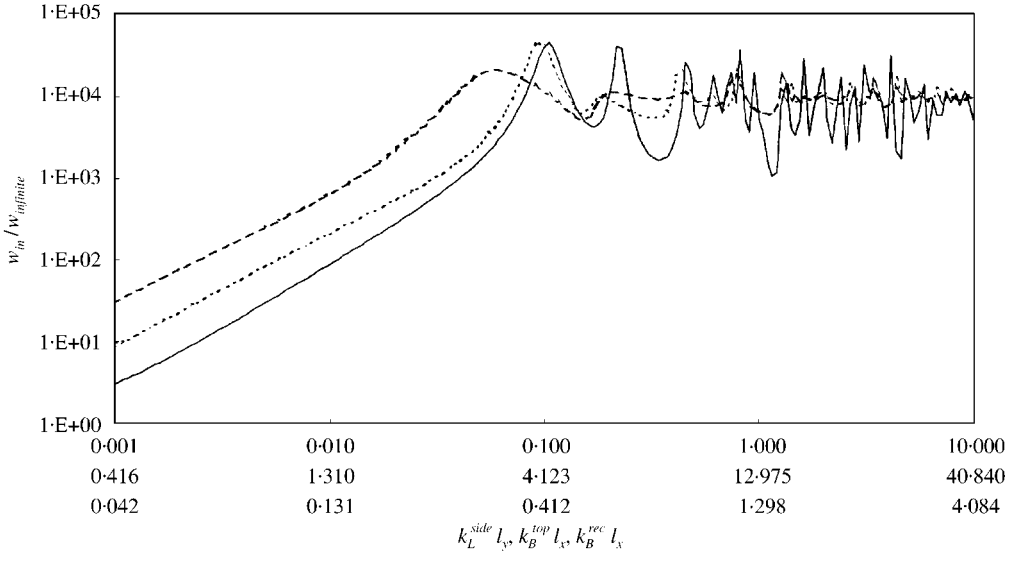

Figure 5. W_{in} for force at $(0{\cdot}5l_x, 0{\cdot}5l_z)$, $l_x = l_y$, $l_z = 2l_y$, $h_{top} = 0{\cdot}02l_y$, $h_{side} = 0{\cdot}02l_y$, η = 1E-4. $W_{complete}$ (—), $W_{Y\Sigma side}$ (- - -), $W_{Y\Sigma all}$ (– – –).

and

$$Q^L = \tfrac{1}{2}\{Y_s^{O\Sigma LL}F^L + Y_s^{O\Sigma UL}F^U\}F^{0*}, \tag{20}$$

respectively. These are analogous to the single-point, single-component case.

For a box of dimension $2l_y$ by l_y and height l_y, constructed of plates of thickness $0{\cdot}02l_y$ and attached to a $2l_y$ thick recipient plate, the complete transmitted input power $W_{complete}$ (that is, the real part of equation (5)) is shown in Figure 5 for a point force positioned at the centre of the top-plate. The estimate obtained assuming a uniform force distribution along each of the side-wall interfaces $W_{Y\Sigma side}$ (i.e., the real part of equation (12)) and the estimate assuming a uniform force distribution around the entire perimeter of the box $W_{Y\Sigma all}$ (i.e., the real part of equation (19)) are also shown. In Figure 6 the imaginary components of the three input powers are presented. In all these Figures, normalization is with respect to the power resulting from a point force applied directly to the recipient plate.

For $W_{complete}$ a stiffness controlled region (associated with deformation of the top-plate) is seen followed by a resonant region. It can be expected that resonances for $k_L l_y < \pi/2$ are only associated with the enclosed area of the top-plate whilst for $k_L l_y > = \pi/2$ the in-plane characteristics of the side-walls will also have an influence. For very high $k_L l_y$ the enclosed area of the recipient plate can also be expected to assume importance.

$W_{Y\Sigma side}$ is seen to overestimate the power in the stiffness region, but to estimate the first three resonances and the overall trend of the power in the resonant region. In the context of the model having application at a preliminary design stage, the prediction of the resonances is considered adequate because their distinct frequencies can be discerned clearly. The observation that the level of the fundamental and the third resonances are captured but that the level of the second is not does indicate a limitation with respect to detailed design work. For such applications the approach could be extended to include additional orders of the force distributions Fourier series. Inclusion of the first order term would, for example, enable the force distribution at the second resonance to be mimicked more accurately and

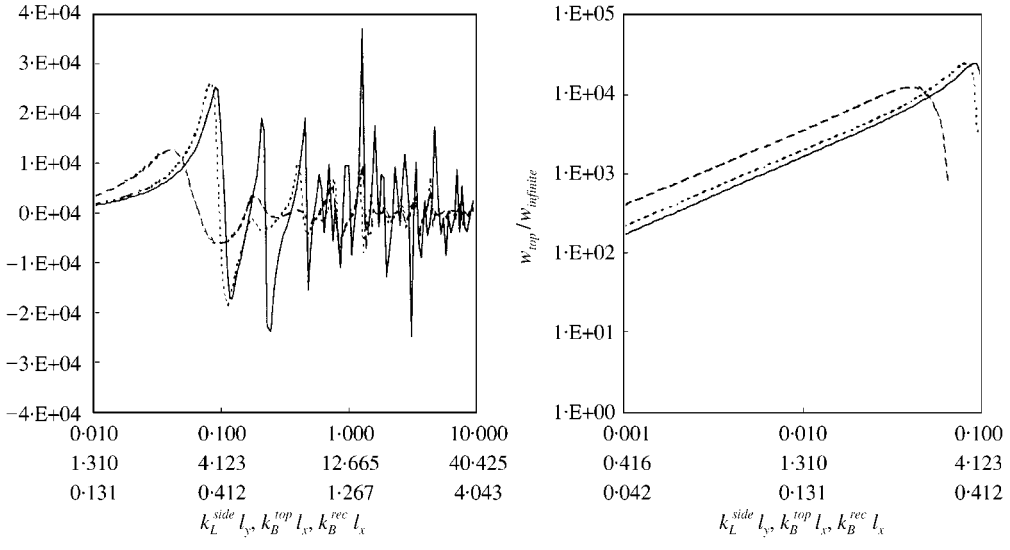

Figure 6. Imag (Q_{in}) for force at ($0{\cdot}5l_x$, $0{\cdot}5l_z$), $l_x = l_y$, $l_z = 2l_y$, $h_{top} = 0{\cdot}02l_y$, $h_{side} = 0{\cdot}02l_y$, η = 1E-4. $W_{complete}$ (—), $W_{Y\Sigma side}$ (- - -), $W_{Y\Sigma all}$ (– – –).

therefore the level at this frequency to be estimated more reliably. The inclusion in the estimate of only the uniform, zero order, component also explains the discrepancy in the stiffness region since at these wavenumbers, the "tails" of many of the higher order components will also make a contribution. Whilst in this "long wavelength" region the limited spatial variations tend to favour a uniform force assumption, an even better estimate would be possible were these "tails" accounted for when determining the level.

For $W_{Y\Sigma all}$ even greater overestimation is observed in the stiffness region and the prediction of the resonances is poorer. However the estimate is reliable with respect to the trend of the power; in particular this is noticeable for $k_L l_y > 1$ indicating that a diffuse wavefield is approached in the top-plate for these wavenumber.

Results for the power transmitted through the lower edge of the box and into the recipient plate are shown in Figure 7. For $k_L l_y < 0{\cdot}1$ (corresponding to the stiffness-controlled region of the input power) it is noted that $W_{Y\Sigma side}$ and $W_{Y\Sigma all}$ both estimate $W_{complete}$ more reliably than for the input power calculation. The reason for this is that the "thick" recipient plate is such that it restrains the deformation of the structure at the lower interface of the box. In contrast to the side-wall/"thin" top-plate interface, the differences between the responses imposed by the estimates and the response of the complete solution are, therefore, similarly restrained. Regarding the estimation of the resonant region, $W_{Y\Sigma side}$ is seen to capture with respect to both magnitude and wavenumber the first resonance but to capture the third resonance only with respect to wavenumber. The second resonance is barely determined at all. This contrasts slightly with that seen for the input power where both the first and third resonances were captured with respect to both magnitude and wavenumber and the second with respect to wavenumber. For $W_{Y\Sigma all}$ the finding is that none of the resonances are reliably estimated. This is in accordance with that seen for the input power. The result that both $W_{Y\Sigma side}$ and $W_{Y\Sigma all}$ are reliable with respect to the overall trend is similar.

The effect of moving the point force to a non-central position introduces anti-symmetric modes into the system. A uniform force distribution is clearly different from any non-symmetric condition and therefore further discrepancies can be anticipated between $W_{complete}$ and the estimates $W_{Y\Sigma side}$ and $W_{Y\Sigma all}$. The real and imaginary components of the

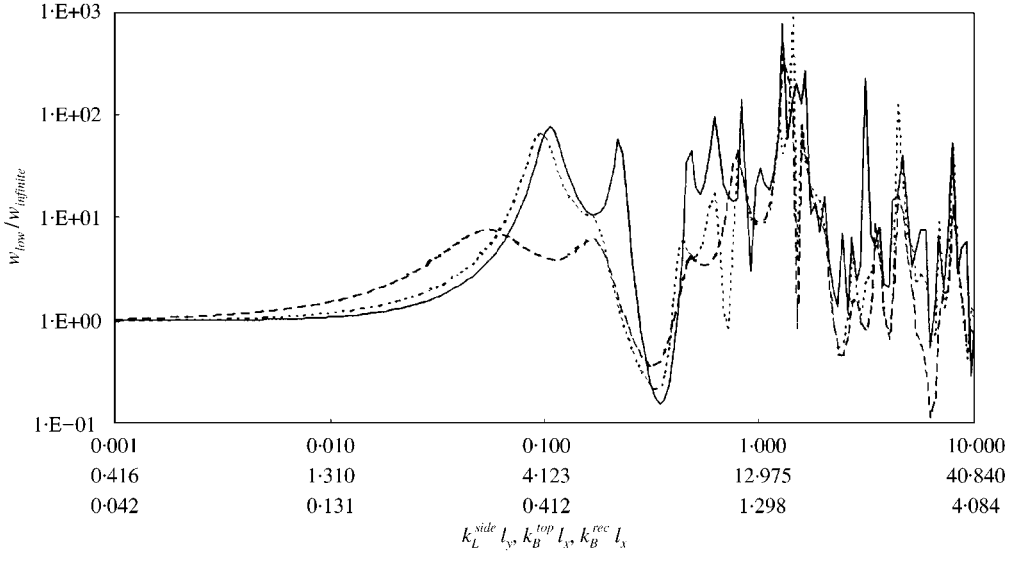

Figure 7. W_{low} for force at $(0{\cdot}5l_x, 0{\cdot}5l_z)$, $l_x = l_y$, $l_z = 2l_y$, $h_{top} = 0{\cdot}02l_y$, $h_{side} = 0{\cdot}02l_y$, $\eta = 1\text{E-}4$. $W_{complete}$ (—), $W_{Y\Sigma side}$ (- - -), $W_{Y\Sigma all}$ (– – –).

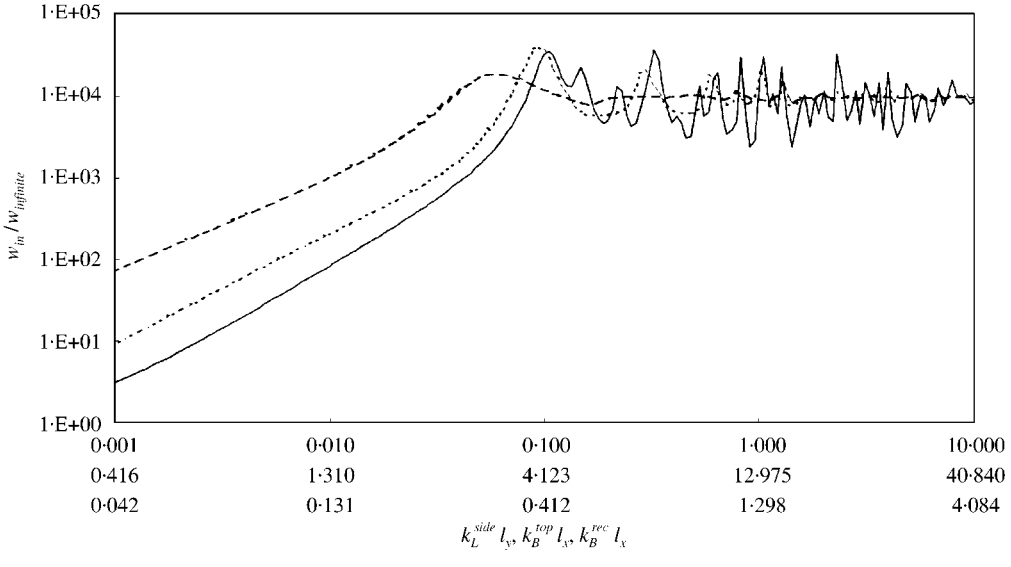

Figure 8. W_{in} for force at $(0{\cdot}4l_x, 0{\cdot}4l_z)$, $l_x = l_y$, $l_z = 2l_y$, $h_{top} = 0{\cdot}02l_y$, $h_{side} = 0{\cdot}02l_y$, $\eta = 1\text{E-}4$. $W_{complete}$ (—), $W_{Y\Sigma side}$ (- - -), $W_{Y\Sigma all}$ (– – –).

input power at $(0{\cdot}4l_x, 0{\cdot}4l_z)$ are shown in Figures 8 and 9 respectively. Compared with the centrally excited case (Figures 5 and 6) it is observed that although further modes, i.e., the anti-symmetric, are indeed evident, the discrepancies between the estimates and $W_{complete}$ are not noticeably larger. Moreover, for broadband excitation, it could be argued that the increased modal density, and thereby increased distribution of vibrational energy amongst more modes, is such that in an overall sense the discrepancies have been reduced.

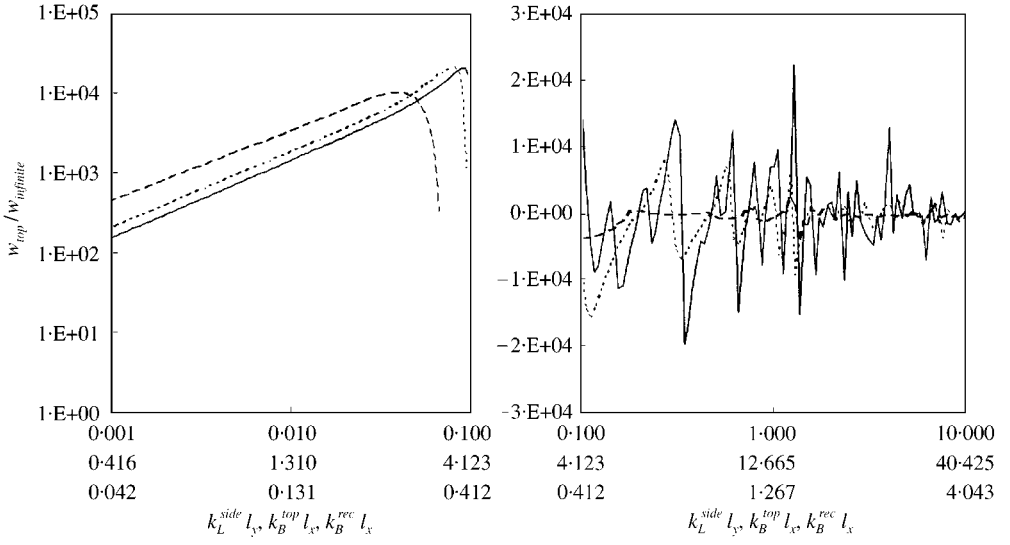

Figure 9. Imag (Q_{in}) for force at ($0{\cdot}4l_x$, $0{\cdot}4l_z$), $l_x = l_y$, $l_z = 2l_y$, $h_{top} = 0{\cdot}02l_y$, $h_{side} = 0{\cdot}02l_y$, η = 1E-4. $W_{complete}$ (—), $W_{Y\Sigma side}$ (- - -), $W_{Y\Sigma all}$ (– – –).

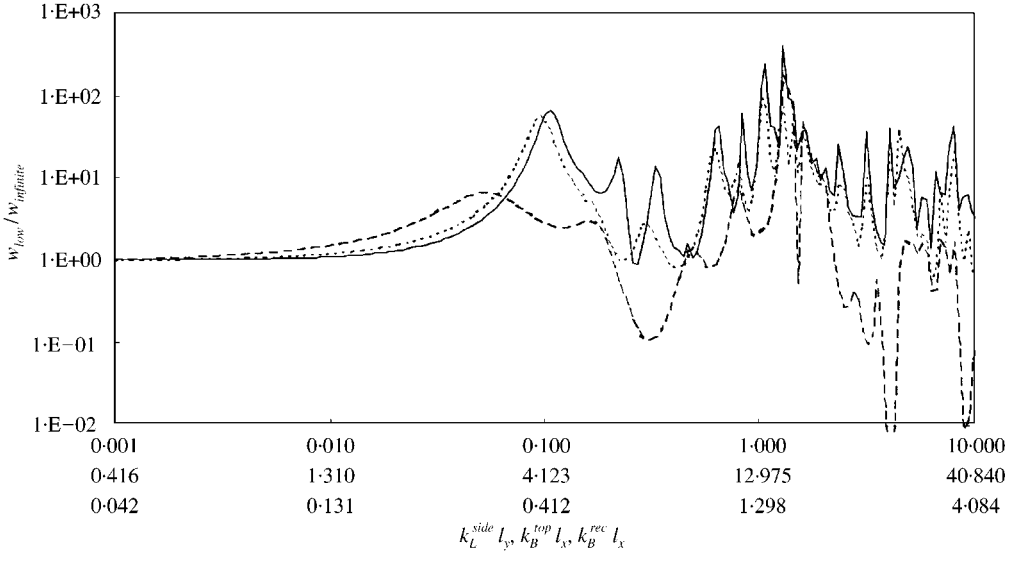

Figure 10. W_{low} for force at ($0{\cdot}4l_x$, $0{\cdot}4l_z$), $l_x = l_y$, $l_z = 2l_y$, $h_{top} = 0{\cdot}02l_y$, $h_{side} = 0{\cdot}02l_y$, η = 1E-4. $W_{complete}$ (—), $W_{Y\Sigma side}$ (- - -), $W_{Y\Sigma all}$ (– – –).

The corresponding result for the power transmitted through the lower interface of the box is shown in Figure 10. As for the input power $W_{Y\Sigma side}$ is seen to capture reliably the stiffness region and the first resonance and the overall trend for higher wavenumbers. The result for $W_{Y\Sigma all}$ is less promising where for $k_L l_y > 1$ there is a tendency for it to underestimate the power. This is not seen for the input power.

If the point force is positioned close to an edge or a corner its character can be expected intuitively to have greater influence upon the force distributions at the nearby edges than at

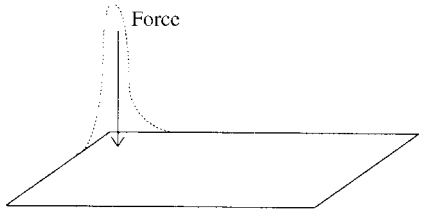

Figure 11. Exaggerated force distribution for point force positioned close to a corner.

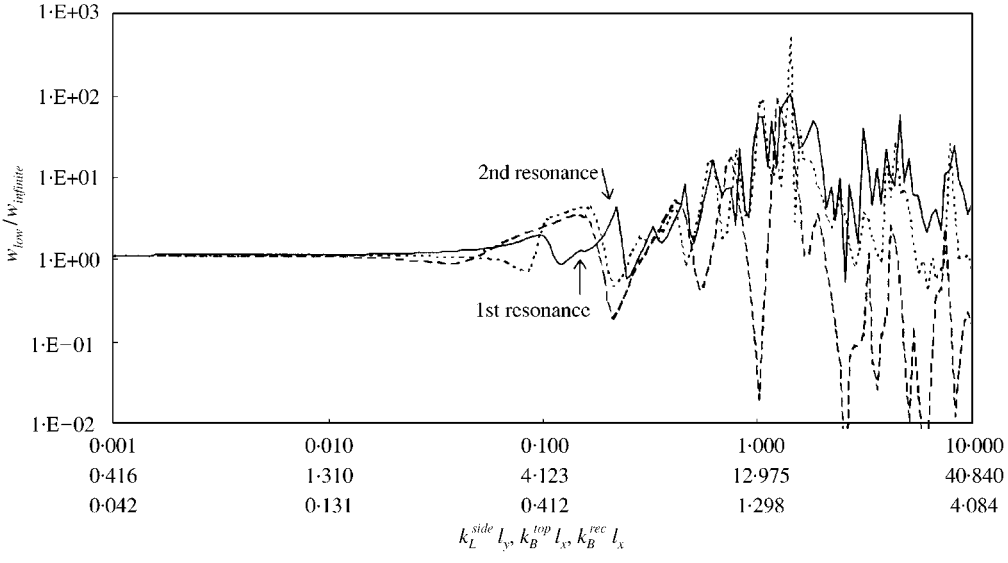

Figure 12. W_{low} for force at $(0{\cdot}1l_x, 0{\cdot}1l_z)$, $l_x = l_y$, $l_z = 2l_y$, $h_{top} = 0{\cdot}02l_y$, $h_{side} = 0{\cdot}02l_y$, $\eta = 1\text{E-}4$. $W_{complete}$ (—), $W_{Y\Sigma side}$ (- - -), $W_{Y\Sigma all}$ (– – –).

remote ones. If, for example, the wavelength is large compared with the distance to the nearest edge then distinctly non-uniform force distributions over the four edges can be expected (see Figure 11). In Figure 12 the power through the lower edge is therefore shown for a point excitation force positioned at the corner $(0{\cdot}1l_x, 0{\cdot}1l_z)$.

In contrast to intuition, the influence of position upon the estimate is only weak and indeed significant only for wavenumbers around the first and second resonances, whereby $W_{Y\Sigma side}$ and $W_{Y\Sigma all}$ have a tendency to overestimate the power. As a consequence of the wavefield being diffuse the influence is negligible for the higher wavenumber. Increased diffusivity at high wavenumbers attenuates this.

Finally, in Figure 13 the power transmitted through the lower edge is shown for a square top-plate with an excitation force at $(0{\cdot}4l_x, 0{\cdot}4l_z)$. As a result of the changed model response $W_{Y\Sigma side}$ is now seen to estimate reliably the first four resonances. $W_{Y\Sigma all}$ reliably estimates the first and the third resonances. For these wavenumbers the response is symmetrical about both of the plane axis with a piston-like action and so a uniform force distribution imposed upon the perimeter constitutes an appropriate approximation (see Figure 14). For larger $k_L l_y$ the discrepancies between $W_{complete}$ and the two estimates are similar to those seen for all the other cases. This is indicative of the modal overlap being similar for both the square and rectangular models.

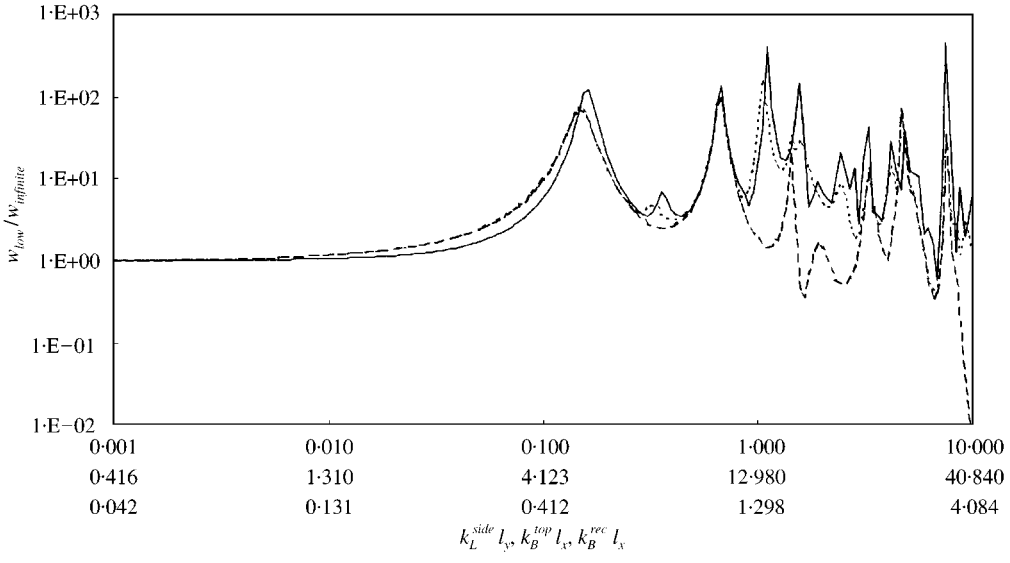

Figure 13. W_{low} for force at $(0{\cdot}4l_x, 0{\cdot}4l_z)$, $l_x = l_y$, $l_z = l_y$, $h_{top} = 0{\cdot}02l_y$, $h_{side} = 0{\cdot}02l_y$, η = 1E-4. $W_{complete}$ (—), $W_{Y\Sigma side}$ (- - -), $W_{Y\Sigma all}$ (– – –).

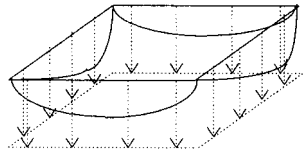

Figure 14. Piston-like action for the first mode of a square plate; (—) velocity distribution, (···) force distribution.

3. COMPARISON WITH EXPERIMENTAL DATA

To corroborate the arguments tested in the study, a comparison can be made with results from an experimental set-up. Whilst, clearly, some discrepancies can be expected due to the simplifications introduced into the model it has also to be considered that discrepancies related to differences in dimension and material parameters are also possible. Consider, for example, the elementary structure of a simply supported plate where its dimensions are composed of thickness (h), l_x and l_y, and its material properties of E, ρ and v. Appreciating that measurement of some or all of these properties are subject to errors implies that small deviations from their true values must be expected. To assess the influence of such "inherent" variations, random errors can be introduced into a numerical model of the plate and a sample population of, for example, the eigenfrequencies,

$$\omega_{mn} = \left(\frac{h^3 E}{12(1-v^2)\rho h}\right)^{0\cdot5}\left[\left(\frac{m\pi}{l_x}\right)^2 + \left(\frac{n\pi}{l_y}\right)^2\right], \tag{21}$$

can be calculated. Hence, for a variation of up to 1% introduced into l_x, l_y, E, h, and ρ (though not v) and a sample population of 2500, probability densities of the plates eigenfrequencies are shown in Figure 15. Significantly, it is seen that only the first two

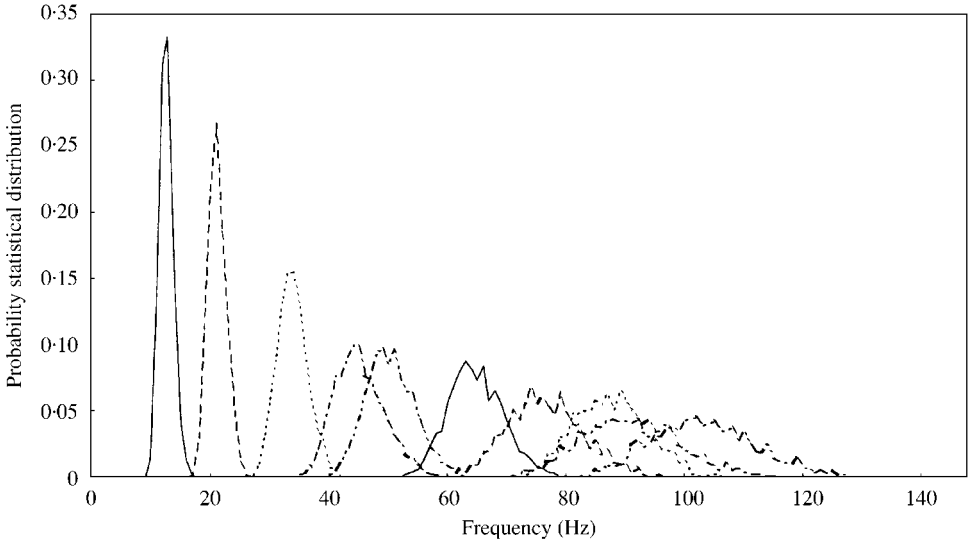

Figure 15. Overlap of eigenfrequencies for simply supported plate when up to 1% variation is introduced into material properties and dimensions.

eigenfrequencies have distinct distributions with negligible overlap. For the third eigenfrequency the distribution has some overlap with the fourth whilst for the fourth and above the overlapping of adjacent distributions is severe. The numerical exercise reveals therefore that for even a notionally simple structure a numerical model can, without a very exact description of the basic dimension and material parameters, only be expected to be reliable up to the first two or three natural frequencies. It can thus be argued that confidence can be assigned to the box model provided that it captures the first/second natural frequencies of a physical system together with the overall trend and any grouping of resonances. Details further than this are deemed too sensitive to the many parameters.

For a Perspex box of dimension 0·27 m × 0·41 m × 0·33 m (all plates 0·01 m thick) attached to a finite recipient plate of dimension 2 m × 3 m (0·01 m thick) the input power for two positions has been measured [6]; position 1 at (0·131 m, 0·197 m) and position 2 at (0·088 m, 0·115 m). Assuming material properties of $E = 6{\cdot}5\text{E}9\ \text{N/m}^2$, $\rho = 1180\ \text{Kg/m}^3$, $v = 0{\cdot}3$ and $\eta = 0{\cdot}05$ (as established from measurement in concurrent work employing Perspex models) the corresponding results from the mathematical model were calculated (see Figures 16 and 17). The discussion begins by comparing the experimental result with $W_{complete}$.

For position 1, the measured response shows a mass-controlled region followed by a stiffness-controlled region and then four distinct resonance groups. Since an infinite recipient plate has been used in the numerical model and a finite plate in the experiment, the experimental result shows a mass controlled region whilst the low-frequency trend of $W_{complete}$ is the characteristic mobility of the receiver. The initial stiffness controlled region leading to the fundamental resonance observed in the experimental result is, however, approximated by the model. Concerning the resonances, the model does not trace the individual peaks but does capture the four distinct groups. The fact that the individual measured resonances are not seen in the model result stems from the simplifications introduced for the boundary conditions of the top plate.

The comparison reveals, therefore, that the very simple model developed has limitations if "accurate" predictions of resonance levels are required, but clear application for preliminarily studies in which only the salient features are needed.

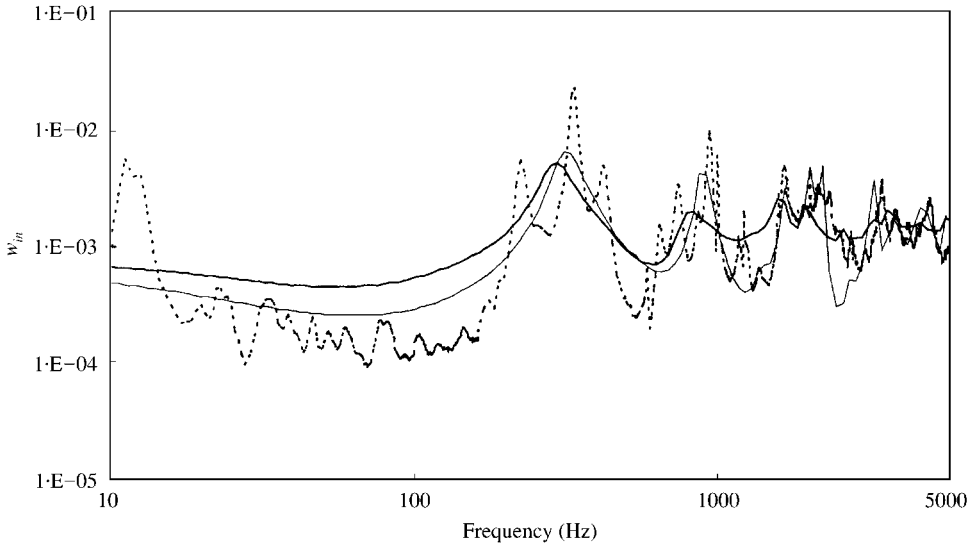

Figure 16. Measured input power (- - -), $W_{complete}$ (—), $W_{\Sigma side}$ (—) and $W_{\Sigma all}$ (—) for Perspex box at position 1 [6].

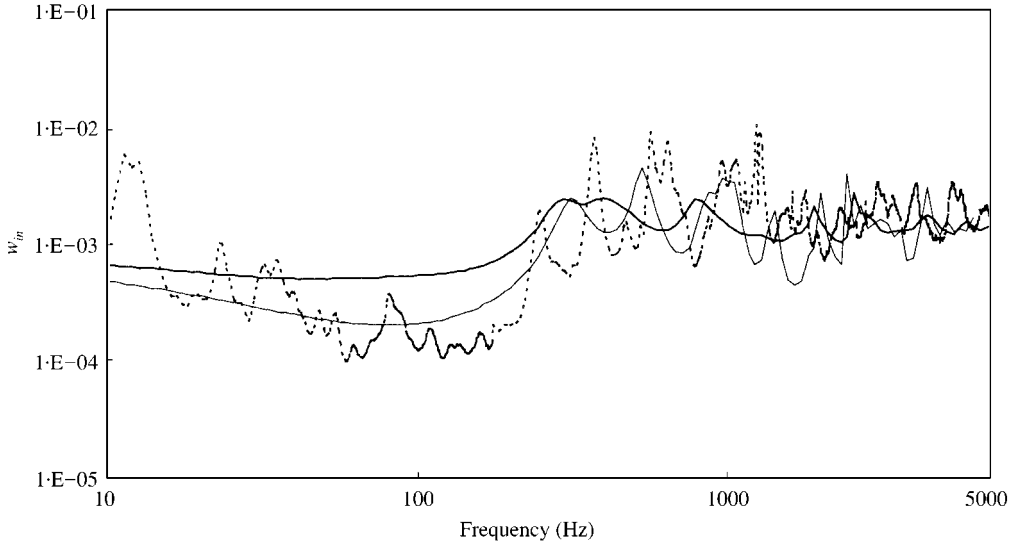

Figure 17. Measured input power (- - -), $W_{complete}$ (—), $W_{\Sigma side}$ (—) and $W_{\Sigma all}$ (—) for Perspex box at position 2 [6].

It is of interest to note that the magnitude of the fundamental resonance is not matched exactly by $W_{complete}$. This reveals that differences exist between the losses in the experimental set-up and those of the mathematical model. However, appreciating the sensitivity of the magnitude of the fundamental resonance to structural losses, together with the inherent difficulties of predicting these at a design stage, it can be argued that the discrepancy is acceptable. The observation that $W_{complete}$ captures the overall trend of the measurement also indicates that for other than strong resonances the moment associated power is "mainly" dissipated within the experimental system.

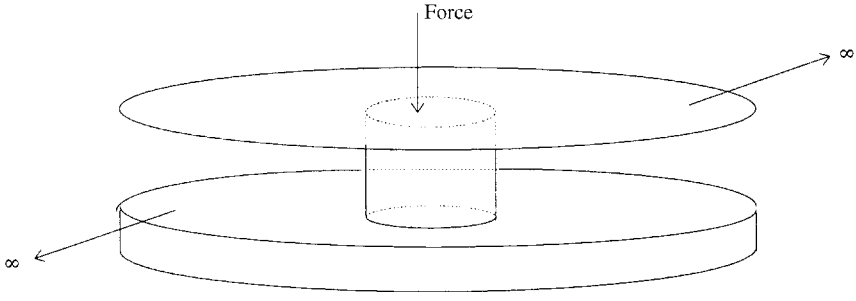

Figure 18. The rectangular "box" converted to a circular "can".

For position 2, $W_{complete}$ mimics the leading stiffness controlled region and the fundamental resonance. Also, the two distinct resonance groups (centred at 500 and 900 Hz) are captured and the overall trend is reliable. This is similar to that seen for position 1. Based upon the comparisons of the two positions, it is suggested that confidence can be assigned to the mathematical model.

For position 1, $W_{Y\Sigma side}$ predicts the leading stiffness-controlled region together with the frequency of the fundamental resonance. It also predicts the frequency of the second resonance together with the overall trend. For position 2, the fundamental resonance is predicted together with the overall trend. The accuracy of the stiffness controlled region and the second resonance is, however, poor.

For both positions $W_{Y\Sigma all}$ does not predict with accuracy the initial stiffness-controlled region nor any of the resonance groups. It is however accurate with respect to the overall trend.

4. A CIRCULAR BOX

Since structures with a circular shape are, compared with rectangular geometries, simpler to describe mathematically it is useful to consider a model of a circular box (that is a "can") and to compare forthcoming results with those from the box. If there is compatibility between the two, the opportunity exists for a greatly simplified model in which the four side-walls are reduced to a simple cylinder. Upon adapting the present model to a circular form by simply "wrapping" the side-walls into a circle (see Figure 18) the input power for three different cans are compared with that for a box in Figure 19. With regard to dimension, Can 1 has a diameter equal to the longest length of the box, Can 2 has the perimeter equal to that of the box and for Can 3 the area of the can and the area of the box are equal. These three criteria were used because they are the most evident ways in which circular and rectangular geometries can be related to each other.

It is seen that none of the three cans capture either the stiffness-controlled region or the fundamental resonance of the box. However, both the "equal perimeter" and "equal length" cans mimic the second and third resonances of the box and both also capture the overall trend at high wavenumbers. Despite differences in signature, all of the models do have the same character for the input power in each case which can be considered to consist of a fundamental resonance, a second resonance, a group of resonances and finally a region characterized by high model overlap.

To assess whether the compatibility between the box and can models is poor in the stiffness region and at the fundamental resonance because of the "extreme" rectangular

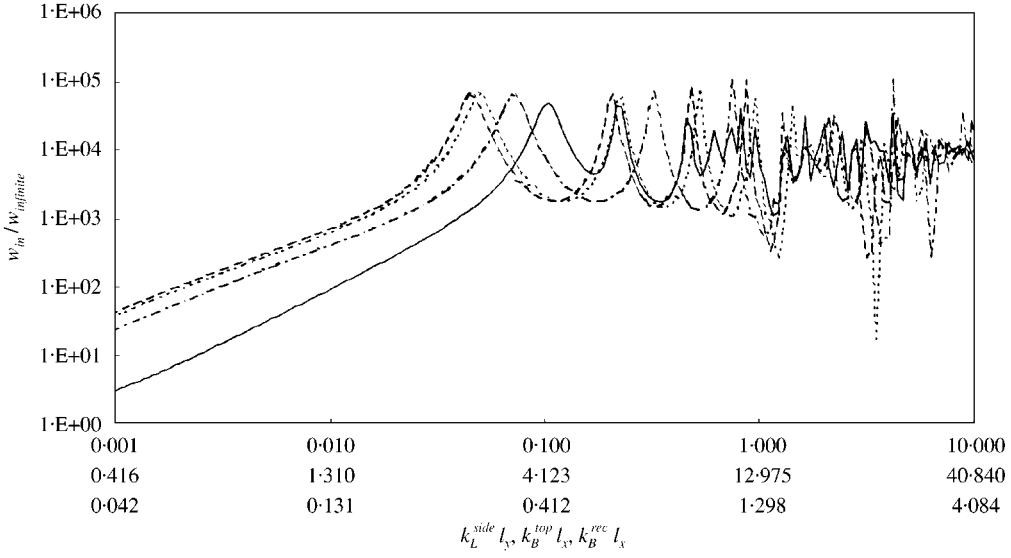

Figure 19. W_{in} compared for can and box. Box (—) for force at $(0{\cdot}5l_x, 0{\cdot}5l_z)$, $l_x = l_y$, $l_z = 2l_y$, $h_{top} = 0{\cdot}02l_y$, $h_{side} = 0{\cdot}02l_y$, η = 1E-4. Can 1 (– – –) for r = length, Can 2 (– – –) for r = perimeter, Can 3 (- - -) for r = area.

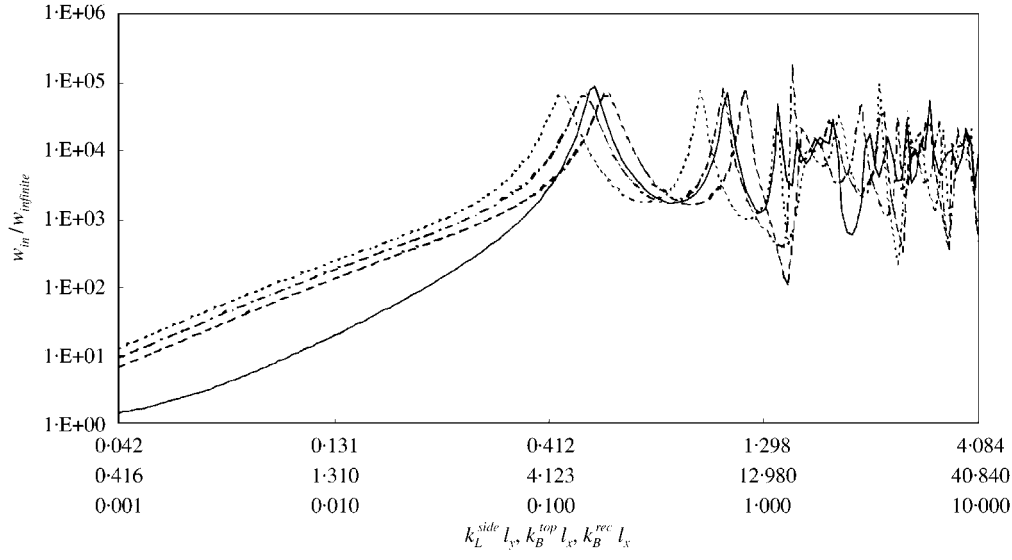

Figure 20. W_{in} compared for can and box. Box (—) for force at $(0{\cdot}5l_x, 0{\cdot}5l_z)$, $l_x = l_y$, $l_z = l_y$, $h_{top} = 0{\cdot}02l_y$, $h_{side} = 0{\cdot}02l_y$, η = 1E-4. Can 1 (– – –) for r = length, Can 2 (– – –) for r = perimeter, Can 3 (- - -) for r = area.

form of the box, results for a square box are also presented (see Figure 20). Though predictions of the fundamental resonance are reliable for the "equal length" and "equal area" cans, those in the stiffness-controlled region are overestimated. For the resonances the observation is, as for the rectangular box, that their character has similar grouping for all models.

5. CONCLUDING REMARKS

With a view to obtain an analytical model suitable for engineering design applications, the vibrational power in box-like structures has been studied. For estimates of the power input into the top-plate and the power transmitted to the recipient plate

- The box can be considered to be constructed of (a) four side-walls each carrying only in-plane waves and each with only elementary "roller" boundary conditions at the vertical edges, and (b) an infinite top-plate only attached to the side-walls with respect to translational forces. This is, because experimental results show that the losses in a "true" box associated with wave conversion and then divergence and dissipation, can agree, approximately, with divergence in the model associated with the power propagating to the outlying region of the infinite top-plate.
- Numerical results show that for frequencies up the second/third resonance, the force distributions along the upper and lower edges of the box can be considered uniform. Provided that the necessary effective strip mobilities are obtained, the model reduces to a problem of eight unknowns. A proviso is that for the input power there is some overestimation of the transmission in the stiffness-controlled region. Also, strongly excited and distinct resonances associated with antisymmetric modes are not captured.
- For frequencies above the fundamental resonance, the overall trend can be captured by assuming that the force distributions around the upper and lower perimeters of the box are uniform. This simplification is also suitable for frequencies where the top-plate exerts a piston-like force distribution; that is, the fundamental frequency for a square top-plate. If the overall effective strip mobilities are obtained this reduces the model to be a problem of only two unknowns.
- For accurate predictions of signature, it seems that a box cannot be simplified to a circular can. Such a conversion can, however, be useful with respect to predictions of the characteristic grouping of the resonances and of the overall trend.
- That the above conclusions are consistent for both a thick recipient plate (the numerical work) and a thin recipient plate (the experimental work) confirms that the thickness ratio is not pivotal for the proposed simplifications. The range of applications in engineering practice is, therefore, large.

ACKNOWLEDGMENTS

The authors are grateful to Dr C. de Jong and Mr F. v. d. Knaap, TNO Institute of Applied Physics, Netherlands for their constructive criticism on the work.

REFERENCES

1. R. A. FULFORD and B. A. T. PETERSSON 2000 *Journal of Sound and Vibration* **232**, 877–895. Assumed uniform force distributions for the estimation of vibrational power in built-up systems involving box-like structures: Part 1.
2. R. A. FULFORD and B. A. T. PETERSSON 1999 *Journal of Sound and Vibration* **227**, 479–510. The role of moments on the vibration transmission in built-up structures.
3. S. H. LIU 1996 *Ph.D. Thesis, University of Southampton*. In-plane and flexural vibration in built-up plate structures.
4. L. CREMER, M. HECKL and E. UNGAR 1973 *Structure-Borne Sound*. Berlin: Springer-Verlag, second edition.

5. P. HAMMER and B. PETERSSON 1988. *Journal of Sound and Vibration* **129**, 119–132. Strip excitation; Part I: strip mobility.
6. C. A. F. DE JONG and F. G. P. VAN DER KNAAP *TNO Institute of Applied Physics*, *TPD-HAG-RPT*-950092. Input and transfer mobilities of a box-like seating structure: experiments and model calculations.

APPENDIX A: NOMENCLATURE

E	Young's modulus
F	force
H	Hankel function
Q	complex power
W	transmitted power
Y	mobility
h	thickness
i	imaginary unit
k	wavenumber
l	linear length
m, n	modal number
p	spatial point
r	radial length
x, y, z	co-ordinates
η	loss factor
v	Poisson ratio
ω	angular frequency

Indices

0	input force position
B	bending wave
L	lower edge of side-wall
N	number of points in the discretization
$O\Sigma$	overall effective mobility
U	upper edge of side-wall
m,n	side plate number
r	recipient plate
s	side-wall
t	top-plate
Σ	effective mobility

Notation

*	complex conjugate